

UNCLASSIFIED

Defense Technical Information Center
Compilation Part Notice

ADP011212

TITLE: Early Light Imaging for Biomedical Applications

DISTRIBUTION: Approved for public release, distribution unlimited

This paper is part of the following report:

TITLE: Optical Sensing, Imaging and Manipulation for Biological and Biomedical Applications Held in Taipei, Taiwan on 26-27 July 2000. Proceedings

To order the complete compilation report, use: ADA398019

The component part is provided here to allow users access to individually authored sections of proceedings, annals, symposia, etc. However, the component should be considered within the context of the overall compilation report and not as a stand-alone technical report.

The following component part numbers comprise the compilation report:

ADP011212 thru ADP011255

UNCLASSIFIED

Early Light Imaging for Biomedical Applications

P. P. Ho¹ and R. R. Alfano

Institute for Ultrafast Spectroscopy and Lasers
Departments of Electrical Engineering and Physics
The City College of The City University of New York, NY, NY 10031

ABSTRACT

Objects located in highly scattering biomedical media can be imaged with sub-millimeter spatial resolution using the early light selected by time, spatial, and polarization gates. Spectroscopic fingerprints can provide diagnostic potentials for medical screening by utilizing fluorescence, excitation, absorption, and Raman approaches.

1. INTRODUCTION

Current tools used by the medical professionals to diagnose diseases rely heavily on X-rays, nuclear radiation, magnetic resonance, chemical analysis, positron emission, and ultrasound. Video and computer imaging have enhanced some of these modalities to detect pathological changes caused by disease. To increase the sensitivity of existing screening techniques (e.g., 75% of women whose mammograms were identified to be positive turned out to be benign after a biopsy) and to reduce possible side effects of X-rays and isotope radiation, new techniques are needed.

Over the past fifteen years, various optical detection and imaging methods have appeared on the scene to measure objects hidden in turbid and biomedical media. Ultrafast lasers and spectroscopy techniques with computer-assisted optical tomography can improve the accuracy of diagnosis. Using an optical Kerr gate¹, the early light was selected to generate clear images¹ of a 0.1-mm width test bar hidden behind a 3.5-mm thick human breast tissue. Using a time gated streak camera method² and high repetition rate 100-fs laser pulse illumination to scan and collect the transmitted signals, the image of a ~ piece of chicken fat of ~ 2.5-mm thickness embedded in a 40-mm thick chicken breast tissue was obtained.

Optical spectroscopy offers a mean for the characterization of physical and chemical changes that occur in diseased tissues. Adding spectral information obtained from fluorescence, absorption, excitation, and scattering in spatial domains with early light imaging optical approaches offer advantages in the minimal invasive approach to identify hidden objects such as cancers in their earliest stage of growth. This presentation focuses on the principle and methods of ultrafast early gating techniques.

2. HISTORY OF EARLY LIGHT IMAGING

When photons travel through a turbid medium, three signal components¹⁻⁴ can be defined: ballistic, snake, and diffusive. A schematic diagram of these three components is shown in Fig.1. Ballistic photons take the shortest path through the medium, while the diffusive scattered light of the incident photons travels over a much larger distance in turbid samples. The snake component arises from those photons scattering within a small forward angular cone which arrives on the onset of the diffusive component. In a thick highly turbid inhomogeneous medium, such as human tissues, the contribution to the ballistic component becomes exceedingly small and is buried and merged into the snake/diffusive component. The early light (ballistic and snake photons) preserves some direct image information.

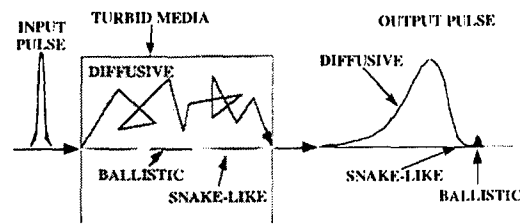


Fig.1 Schematic of ballistic, snake, and diffusive signal of an ultrashort laser pulse propagating through a turbid medium. Ballistic: coherently forward scattered

Several schemes have evolved over the years to sort out the image-bearing ballistic and snake photons from the multiple-scattered diffuse photons. Beside the use of an ultrafast time shutter, these schemes exploit one or more of the changes that scattering induces on the characteristics such as directionality, polarization, coherence and temporal duration of the incident light. Since, the image-bearing photons change the least, the idea is to devise a *gate* that will let the photons with a specific initial property through but block others. One such scheme is a *space gate* that exploits the fact that the ballistic and snake photons come out of the tissue in the incident direction, while the multiple-scattered light emerges in all directions. A small aperture centered on the direction of incidence and placed after the sample will collect the on-line-transmitted light and effectively discriminate against a significant fraction of the scattered light. Similarly, a *time gate* capitalizes on the fact that image-bearing photons emerge from

¹ Correspondence: Email: ho@photonicsmail.sci.cuny.cuny.edu Telephone: 212 650 6808; Fax: 212 650 5530

the sample sooner than the diffusive photons. For early light imaging, one then needs a shutter that will open for a short duration, typically a few picoseconds, to let the early photons through and then close in time to leave out the delayed scattered photons. Similar gating schemes based on polarization and coherence of light have also been devised. Often a single gate may not be discriminating enough. A space gate cannot filter out the photons that have first been scattered out of the incident direction and then back into it. A time gate employed after the space gate can cut out such "on-line" scattered photons, since the scattering makes them travel longer distances and emerge out of the sample later than the ballistic photons that propagate straight through.

Several other groups have pioneered in early light imaging techniques. A photon counting based delayed coincidence detection technique⁵ was developed to detect the internal structures inside turbid media. Using ps diode lasers⁶ and a 120-ps early light time-gating, a large tumor embedded in a thick breast tissue was identified. Reintjes et al used the nonlinear gain from stimulated Raman scattering⁷ to enhance the quality of optical images in scattering media. Chance et al⁸⁻¹¹ has demonstrated an optical imaging system using the streak camera technology to study the deoxyhemoglobin in brain with a simulation system. Coherent imaging (time-resolved holography) was measured^{12,13} using the principle of the pulse holographic interference technique. A holographic image is formed from the coherent (ballistic) part and is separated out from the incoherent (diffusive) part which takes a longer path and contributes a uniform noise background. Diffusive optical tomography using second harmonic nonlinear correlation detection has also been demonstrated¹⁴⁻¹⁶. An e^{-32} factor attenuation of femtosecond input signals through turbid media has been observed. Imaging quality can be improved by reducing the diffusive component using absorption and fluorescence-absorption techniques^{17,18}. Results based on the ps time-of-flight and absorption change,¹⁸ the image of the internal structure of rats in vivo was obtained.

3. TIME GATES

An ideal ultrafast shutter for early light imaging desires the \sim ps or fs time resolution, fast (\sim ps) triggering response time and jitter, low gate temporal fluctuation ($< 1\%$), high (\sim GHz) repetition rate, large dynamic range ($> 10^{10}$), wideband (200-nm to 5,000-nm) spectral sensitivity, large acceptance angle, low operation power, small geometrical dimension, good environmental stability, easy operation, and low cost.

3.A Electronic Controlled Time Gates

Gated Image Intensifier: The image intensifier is an electro-optical device which can detect and intensify 2D optical images from the near uv to the near IR wavelength regions. A microchannel plate (MCP) image intensifier uses an MCP to convert incident photons into electrons with $\sim 10,000$ times gain. An MCP consists of arrays of millions of glass capillary coated with second-electron-emission materials to amplify the electron signal current produce from an image sensor (photocathode). For a gated image intensifier, the time gated function is added by introducing an electronic gate voltage pulse to the amplification photocathode. A gated image intensifier¹⁹ is used as an ultrafast time shutter with an opening time (FWHM) of ~ 80 -ps.

Streak Camera: In this method, signal photons are focused onto a photocathode through a thin slit. After the emitted photoelectrons from the cathode are accelerated through an anode, these electrons are deflected by an applied voltage ramp which increases with time and streaks the electrons onto a phosphor screen to be displayed. These electrons which are released at different times and arrived the phosphor screen at different spatial locations with a phosphorescent track can be recorded by a CCD camera. Only one-dimensional signals can be imaged. The minimum time resolution of a streak camera is ~ 1 -ps.

3.B Nonlinear Optical Time Gates

Optical Kerr Gate (OKG): OKG is based on the third order (χ^3) nonlinear optical process and has similar design parameters as a regular camera shutter and can also be used to gate incoherent optical signals. All other three types of nonlinear optical gates listed below require the phase matching condition and are limited to coherent signals only. Two optical beams are needed in an OKG. One beam is used as the gating beam and the other is used as the probing beam. The intensity of the probing pulse should be kept to be small in compared to the gating pulse. A Kerr medium is situated between a pair of crossed polarizers. The gating pulse induces a transient birefringence in a Kerr medium and causes the polarization change of the probing beam. To prevent the "coherent artifact" in an OKG, the wavelength of the probing beam should be different from the gating beam. To avoid the saturation effect²⁰ and the nonlinear absorption²¹ in a Kerr medium, the gating pulse intensity at the Kerr cell should be set to be < 1 GW/cm² for a 1-cm long CS₂ Kerr medium. The time delay between the gating and probing pulse is controlled by a stepping-motor with a minimum temporal resolution to be \sim fs. The minimum temporal resolution of an OKG is ~ 100 -fs which is limited by the gating pulse duration (~ 100 -fs) and the response time of the gating material (< 10 -fs for glass).

Optical Parametric Amplified Gate (OPAG): OPAG²² is based on the second order nonlinear optical process (χ^2). When an intense gating laser pulse at frequency ω_1 and a weak signal beam at ω_2 ($\omega_2 < \omega_1$) co-propagate in a χ^2 material, the output signal under the phase matching condition can be gated and amplified. The intensity of the output idle signal is proportion to a function of $\sinh^2 [\frac{1}{2} GL]$, where L is the interaction length of the χ^2 material and G is a gain parameter ($\sim I_{\text{gate}} \times \chi^2$). Using a 22-mm long KTP gating material and a 10-mJ 532-nm 30-pJ gating pulse, a time-gated signal at 1064-nm with a $> 1,000$ gain factor can be obtained (see SPIE #4082-46).

Up-Conversion Gate (UCG) and Second-Harmonic Auto-Correlation Gate (SHAG): The up-conversion uses a χ^2 NLO process.

The major difference between UCG and OPAG is the output signal frequency used in UCG, ω_s , is equal to the sum of the gating frequency and incident signal frequency ($= \omega_1 + \omega_2$). While in OPAG, the output frequency, ω_s , is equal to the difference of the gating frequency and incident signal frequency ($= \omega_1 - \omega_2$). SHAG is a special case of UCG where both the gating frequency and incident signal frequency are equal ($\omega_1 = \omega_2 = \omega$). The output signal frequency $\omega_s = 2\omega$. The minimum temporal resolution from both UCG and SHAG is in the fs region which is limited by the time convolution of the gating pulse and the signal pulse. Based on the output frequency is increased (up) or decreased (down), the output signal from UCG or OPAG will be either a function of $\sim \sin^2[\frac{1}{2}GL]$ or $\sinh^2[\frac{1}{2}GL]$. The maximum possible output signal from a UCG is always less or equal to the incident signal. While from the PAG, the output signal can be exponentially grown to the limitation \sim the gating pulse energy. The advantage of a UCG is that when the incident frequency ω_2 is in the infrared region where the detector sensitivity is poor, using a proper gating frequency, the output signal frequency ω_s can be shifted to the visible region with improved sensitivity and S/N.

Four-Wave-Mixing Coherence Gating: Optical coherent imaging (OCI),^{14,15} holographic methods,^{12,13} four-wave mixing (FWM) gate,²³ and coherent anti-Stokes Raman scattering (CARS) gate⁷ are different four-wave mixed gating techniques. In all of these gating methods, phase matching or coherence conditions are required. The advantages of these methods are good temporal resolution and the flexibility of optics from the combination of four-waves. However, all these methods are suffered to the lower sensitivity. The interference between image-bearing photons and a reference beam derived from the same initial pulse of light forms the mechanism for selective detection in coherence techniques. Photons that are coherent with the reference pulse give rise to a gated signal, while diffusive light does not. The coherence time of the reference pulse determines the duration of the gate. OCI systems are based on interferometry with low-coherence light. In an interferometer, a beam of light is split into two parts and are recombined after they travel two different paths. The two beams form an interference pattern only when they are coherent that is the phase difference between the two remains fixed. If one of the beams interacts with a scattering medium only the ballistic photons will retain their original phase and interfere with the reference beam. Diffusive component loses its original phase and cannot interfere. Interference thus filters out image-bearing ballistic photons and a fraction of snake photons. Light retro-reflected from different depths within the sample are measured by scanning the axial position of the reference mirror and simultaneously recording the interferometric signal amplitude. The two beams interfere only when the two arm path lengths match within the source coherence length. A broadband light source such as super-luminescence diodes with short coherence length, typically $\sim 10 \mu\text{m}$, is used in OCT systems. The longitudinal position of the image can be determined with high-resolution. By scanning the sample beam along the transverse dimensions and performing a longitudinal scan at each position, a two-dimensional image can be obtained.

3.C Equivalent Time Gates: Space, Polarization, and Absorption

Based on spatial arrangements and polarization properties, image information with an equivalent time gated properties can be obtained. These gates can be coupled with an ultrafast time shutter either as described in sections 3A and 3B to achieve higher S/N for a sophisticated imaging instrument or sometimes be used alone for a compact low-cost early light screening tool.

Space Gating Collimator imaging²⁵ and Fourier spatial filtering^{26,27} are two commonly used space gating techniques. In confocal imaging, an optical fiber collimator shines light on the sample and an on-line receiving fiber collimator that faces the transmitter collects the light that passes straight through. Since, the diameter of the collecting fiber is small, it only accepts ballistic light and rejects off-axis scattered light. A two-dimensional image can be formed point by point by scanning the illuminator and collector fibers synchronously across the object while keeping them precisely aligned.

In a Fourier gate, a collimated beam shines the object and a lens of focal length F placed at a distance F focuses the photons that retain their collimation at a distance of $2F$ from the object. The angular spatial frequencies of scattered light will be forward Fourier transformed to the Fourier spectral plane²⁷. The central pattern arising from the collimated portion of the transmitted light represents the zero frequency (DC) component. The intensity of the region spread around the central part represents higher spatial frequencies. Higher angular frequencies are of larger radii. The earlier and the later diffusive signals can be spatially filtered and separated out. A small aperture placed at the focus of the lens transmits the image-bearing light and rejects most of the diffusive component. For example, a hidden object with dimensions of ~ 0.1 to 1-cm embedded in a turbid medium consisting of scattering particles with dimensions ~ 1 to $10\text{-}\mu\text{m}$. The Fourier spatial frequency ($\sim 1/\text{object size}$) of the object is much smaller than that from the surrounding small random particles to be separated.

Kerr-Fourier Time-Space Gate

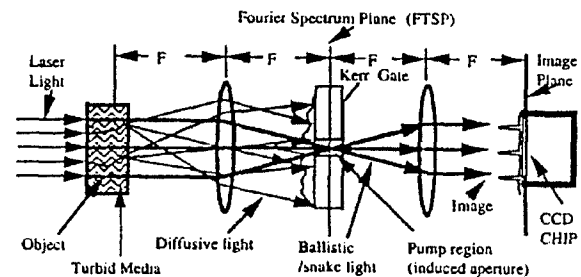


Fig.2 Schematic diagram of early light Kerr-Fourier gated imaging.

Mode-locked laser is used for the gating and probing source. The probing beam is used to illuminate the sample. The gating beam is used to open the Kerr gate. The Kerr cell is set at the back focal plane of the Fourier transform lens and is situated between a pair of crossed polarizers (not shown here). For the Fourier imaging measurement of the object, the second lens L_2 is located at one focal length away from the FTSP and the CCD camera was located at one focal length from L_2 as the $4F$ imaging system.

For most biomedical imaging applications, a large dynamic range of $\geq 10^{10}$ is needed to obtain image information of an object embedded in thick turbid media, such as tumors in breast tissues. A simple time-gating approach may not achieve the required dynamic range. A Fourier spatial filtering technique²⁷ coupled with ultrafast time gating has the capability to improve the dynamic range and S/N. A schematic diagram of early light Kerr-Fourier gated (KFG) imaging is shown in Fig.2. The spatial dimension of the gating laser pulse radial profile can induce a spatial aperture of a given diameter at the Kerr cell to effectively remove the higher spatial frequencies. In this manner, information from the surrounding random small particles can be removed while the lower spatial frequency from the object is transformed. This KFG imaging can detect phantoms in a 70-mm thick 2% intralipid solution with better than 1-mm resolution. The feasibility of constructing a three-dimensional tomographic image was demonstrated by combining two-dimensional shadowgrams formed with a KFG using a back-projection algorithm on a personal computer.²⁸

Polarization Gating The polarization gate makes use of the fact that scattering events depolarize an incident beam of linearly polarized light so that ballistic photons retain their polarization state while the multiple-scattered photons are depolarized. In practice a polarization gate is implemented by shining the object through a linear polarizer and collecting the emerging light through a second linear polarizer. The degree of polarization, defined as $(I_p - I_s)/(I_p + I_s)$ where I_p and I_s are transmitted intensities with the axis of the second polarizer parallel and perpendicular to that of the first respectively, of the transmitted light is used to select the image-bearing component since it is ideally expected to be unity for ballistic light and zero for completely depolarized light. Time-dependent²⁹ polarization status of an optical pulse propagating through a scattering medium is shown in Fig.3. The depolarization coefficient (D) of an ultrashort polarized laser pulse at 532-nm propagating through a suspension of 200-nm diameter polystyrene micro-spheres in water was measured by a streak camera. The suspension was placed in a 50-mm thickness water cell and the scattering length is 4-mm. The measured D values of the ballistic component and the later arrived diffusive component were ~ 1 and 0, respectively.

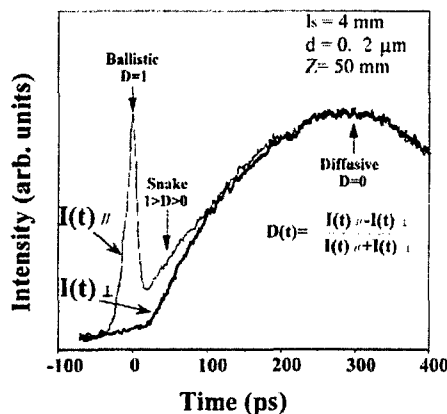


Fig.3 Time-dependent polarization status of optical pulse propagating in scattering media.

Absorption Gating For the fluorescence imaging of an object embedded in a host turbid medium, absorption can reduce the amount of multiple scattered diffusive photons by shortening the optical path of the signal light propagating through the host.¹⁷ The image quality of an object could be improved when it is viewed in the overlapping spectral region between the luminescence spectrum of the object and the absorption spectrum of the surrounding medium.

4. EARLY LIGHT SPECTROSCOPY IMAGING

Optical spectroscopies³¹ can be employed to show the spectral differences caused by the change of the concentration, biological and ionic characters, chemical composition of bonds, organic materials and biological samples.

Diagnosis of Cancer Tissues: The visible fluorescence spectra and relaxation time from cancerous and normal rat kidney, bladder, and prostate tissues show different spectra characteristics. The line of research using fluorescence and excitation spectra was extended to human lung and breast normal and cancerous tissues³². The fluorescence spectral profiles from normal human tissues were found to peak at about 520 nm, often with complex structures. For breast tissues, cancerous fluorescence profiles were smoother and the peak was shifted. The natural fluorophor responsible for the main signature appears to be flavin. It is believed that the absorption from oxy-hemoglobin may be the marker responsible for the spectral structure using visible excitation. Using uv sources, basic molecules, such as NADH, elastin, and collagen in tissues can be excited and used as fingerprints of materials.

Atherosclerosis Diagnosis: Atherosclerosis is a major medical problem for the middle-aged and elderly, and X-ray visualization of arteries following an injection of radio opaque material via a catheter is the common method of diagnosis. Thus, optical spectroscopy offers a means to determine whether a given arterial wall is diseased. Once the plaque is located by spectroscopy, an intense laser can ablate the plaque. Too much plaque or tissue removal can produce perforated arteries. Normal and diseased samples exhibit two peaks near 550 and 600 nm. The intensity of the 600 nm peak was smaller than the 550 nm peak in the diseased samples. The valley between the peaks at 580 nm was used to normalize the spectra from the tissue. The ratio of intensity at 600 nm to 580 nm for a normal artery was 2 and for a diseased artery was unity.³³

Raman Spectroscopy: The molecular components of human tissues are principally composed of proteins, nucleic acids, and lipids. These molecules have characteristic vibrations which can be accurately characterized by Raman spectroscopy. The number of Raman active mode will most likely be altered when the molecular structures change from normal to abnormal states. Raman spectroscopy can be used to analyze these changes on a molecular scale. Visible Raman and fluorescence spectra from 500 nm to 700 nm of human cancerous and normal breast tissues excited at 488 nm have shown noticeable spectral differences. These differences most likely arise from the presence of hemoglobin. A significant difference between the two spectra is the presence of narrow spike-like bands atop the broad band in normal tissue spectra which are absent in cancer. These narrow

spike-like bands arise from Raman scattering spectral lines which was confirmed by changing the excitation wavelengths from 488 nm to 514.5 nm. By comparing the locations in wave numbers of the narrow spike-like bands of the normal breast tissue spectra, we conclude that these narrow bands arise from Raman scattering. The Raman lines are shifted by about 1036, 1242, 1584, 2745, and 2944 cm^{-1} from the laser lines. The normal breast tissue spectrum had two subsidiary maxima located at 556 nm and 592 nm, while no additional maxima were recorded in cancerous breast tissue.

In most biological tissues a large fluorescence emission inhibits the observation of Raman spectral lines. To eliminate the fluorescence background, one must excite and measure Raman spectra in the IR spectral region where fluorescence is much weaker than that in visible spectral region³⁴. NIR Raman scattering spectra of benign breast tissue, benign tumor and malignant tumor breast tissues were measured. From the vibrational modes of the CH_2 , amide, and protein bonds, intense Raman lines were located at ~ 1078 , 1300, 1445 and 1651 cm^{-1} for benign breast tissues; ~ 1240 , 1445 and 1659 cm^{-1} for a benign tumor; and ~ 1445 and 1651 cm^{-1} for a malignant tumor. There were differences in both the number of Raman lines and the intensity ratio among different Raman lines.

A combined Fourier space and polarization gated spectral imaging to sort out early arrived imaging bearing photons of biomedical samples was demonstrated. 2D transillumination spectroscopy images¹⁹ of in-vitro human breast tissue specimens were recorded by an InGaAs NIR camera using 1225-1300 nm light from a forsterite laser. Near-resonant images of a 28mmx12mmx10-mm human breast tissue sample comprising adipose and fibrous tissues were measured with 1225-nm laser and non-resonant images of the same sample were obtained using a 1285-nm laser. These results demonstrate that an appreciable spectroscopic difference may significantly enhance the contrast between different types of early light images from breast tissues.

For the spectral polarization imaging, light from an appropriate white light or low-power laser sources can be used to illuminate the sample. The illumination wavelength is selected by band pass filters located on a multiple filter wheel which can be rotated to the desired filter position by computer control to select the appropriate NIR wavelength. Images can be recorded for the implementation of the scattering (the illuminating and detecting wavelengths are the same) and emission (the detecting wavelengths are different from the illuminating wavelength), respectively. Since the scattering and emission properties of the tissues and tumors are different, both scattered and emitted NIR light images can be used to identify tumors. For polarization difference imaging, the analyzer is kept in a direction while polarizer for illumination is alternatively placed in the parallel and perpendicular polarization directions in respect to the analyzer. Two polarization images will be obtained when the polarization direction of the analyzer is parallel or perpendicular to that of polarizer. The parallel and perpendicular images are used to investigate the surface and inter structures of tumors, respectively. The polarization difference image is obtained by subtracting the perpendicular image from the parallel image. For excitation difference imaging, at least two different wavelengths are used for illumination while a same detection wavelength or wavelength region is used for recording the fluorescence images. Two or more fluorescence images will be obtained with different excitation wavelengths. The excitation difference image can be obtained by subtracting one image from another. For emission difference imaging³⁵, at least two different detection wavelengths are used for recording the fluorescence images while a same excitation wavelength is used for illuminating. Two fluorescence images of a luminous object (1-mm diameter chicken breast tissue stained by Cardio Green) located 31-mm underneath the surface of a host chicken breast tissue illuminated by a 630-nm mode-locked ps laser source was measured at 790-nm and 830-nm as shown in Fig.4a and 4b, respectively. The emission difference image of Fig.4c was obtained by subtracting Fig.4a image from Fig.4b. The image visibility enhancement from the difference imaging can be attributed from the reduction of host tissue emission and diffusion processes.

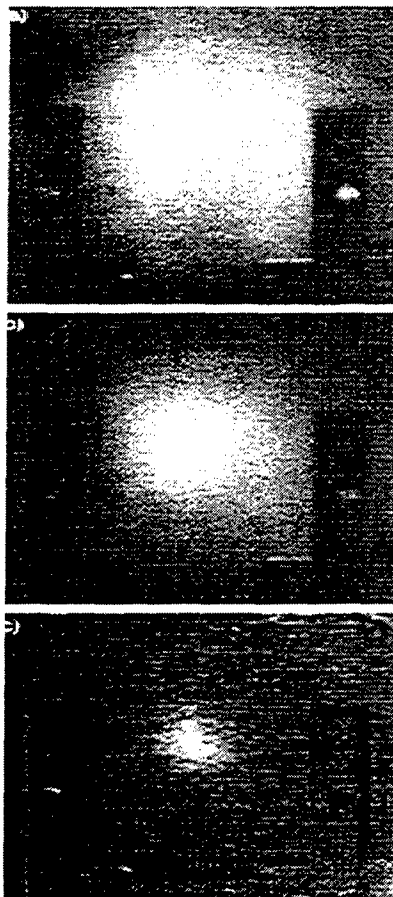


Fig.4 Difference fluorescence imaging of a small piece stained tissue inside a 6cmx5cmx4cm chicken breast tissue. Black U-image is the sample holder.

5. SUMMARY

Photonics can play an important role in today's and tomorrow's biomedical technology for screening and surgical applications. Imaging through a thick highly scattering biomedical sample remains to be a challenge problem. Pico and femtosecond laser sources which are the key element for the early light imaging technique are becoming reliable and compact in size. Early light imaging can be implemented in a number of clinical applications for screening such as prostate cancer, breast cancer, cervical cancer, glaucoma, macular degeneration, macular edema, and atherosclerosis plaques. Understanding of the spectroscopic information from the photonic technology will be the key factor toward the success of disease diagnosis.

ACKNOWLEDGMENT

This research is supported in part by grants from NASA/IRA, NASA/FAR, DoE Center for Excellence in Laser Medicine, U.S. ARMY Medical Research Acquisition Activity, CUNY/CAT NY State Science & Technology Foundation.

REFERENCES

1. L. Wang, P. Ho, C. Liu, G. Zhang, R.R. Alfano, "Ballistic 2-D imaging through scattering walls using an ultrafast Kerr gate", *Science*, **253**, 769-771 (1991)
2. B. Das, K. Yoo, R. Alfano, "Ultrafast time gated imaging in thick tissues", *Optics Letters* **18**, 1002-4 (1993)
3. K. Yoo and R. R. Alfano, "Time-resolved coherent and incoherent components of forward light scattering in random media", *Opt. Lett.* **15**, 320-322, (1990)
4. R. R. Alfano, X. Liang, L. Wang, P. Ho, "Time-resolved imaging of translucent drops in highly scattering medium", *Science* **264** 1913-5 (1994)
5. S. Anderson-Engels, R. Berg, S. Svanberg, O. Jarlman, "Time-resolved transillumination for medical diagnosis", *Opt. Lett.* **15**, 1178-1180 (1990); "Effects of optical constants on time-gated transillumination", *J. Photochem. Photobiol.* **B16**, 155-167 (1992)
6. R. Berg, O. Jarlman, S. Svanberg, "Medical transillumination using short-pulse diode lasers", *Applied Optics*, **32** (1993)
7. M. Duncan, R. Mahon, L. Tankersley, J. Reintjes, "Spectral and temporal characteristics of spontaneous Raman scattering in the transient regime", *Opt. Lett.* **16** 1868-1670 (1991)
8. B. Chance, J. Leigh, J. Miyake, D. Smith, S. Nioka, R. Greenfield, M. Finander, K. Kaufmann, W. Levy, M. Young, P. Cohen, H. Yoshioka, R. Boretsky, "Comparison of time-resolved and un-resolved measurements of deoxyhemoglobin in brain", *Proc. Nat. Acad. Sci.* **5**, 4971-4975 (1988)
9. B. Chance ed. "Photon Migration in Tissues", Plenum Press, NY (1990)
10. E. Sevick, N. Wang, B. Chance "Time dependent photon migration imaging", *SPIE*, **1599** 274-283 (1992)
11. "Photon migration and imaging in random media and tissues", B. Chance, R. Alfano, ed. *SPIE*, **1888** (1993)
12. K.G. Spears, J. Serafin, N.H. Abramson, "Chron-Coherent Imaging for Medicine", *IEEE Trans. Biomed. Eng.* **36** 1210-1221 (1989)
13. H. Chen, Y. Chen, D. Dillworth, E. Leith, J. Lopez, J. Valdmanis, "Two-dimensional imaging through diffusing media using 150-fs gated electronic holography techniques", *Opt. Lett.*, **16** 487-489 (1991)
14. J. Fujimoto, W. Drexler, U. Morgner, F. Kartner, E. Ippen, "Optical coherence tomography", *Optics & Photonics News*, pp25-31, Jan. (2000)
15. J. Fujimoto, S. De Silversti, E. Ippen, R. Margolis, A. Oseroff, "Femtosecond optical ranging in biological system" *Opt. Lett.* **11**, 150-152 (1986); *Science*, "Optical coherence tomography" **254**, 1178-1182 (1991).
16. K. Yoo, Q. Xing, R. Alfano, "Imaging objects hidden in highly scattering media using femtosecond second-harmonic-generation cross-correlation time gating", *Opt. Lett.*, **16** 1019-1021 (1991)
17. K. Yoo, Z. Zang, S. Ahmed, R. Alfano, "Imaging objects hidden in scattering media using a fluorescence-absorption technique", *Opt. Lett.*, **16** 1252-1254 (1991)
18. D. Benaron, D. Stevenson "Optical time-of-flight absorbance imaging of biomedical media" *Science*, **259** 1463-1466 (1993)
19. S. K. Gayen and R. R. Alfano "Sensing lesion in tissues with light", *Optics Express* **4** 475-480 (1999)
20. P. Ho and R. Alfano, "Oscillatory optical induced Kerr kinetics in nitrobenzene", *Opt. Comm.* **30** 428-430 (1979)
21. P. Ho, P. Lu, R. Alfano, "Time-dependent multi-photon absorption in liquids", *J. Chem. Phys.* **74** 1605-9 (1980)
22. J. Watson, P. Georges, t. Lepine, B. Alonzi, A. Brun, "Imaging in diffuse media with UPAG", *Opt. Lett.*, **20** 231-233 (1995)
23. A. D. Sappey, "Optical Imaging through turbid media with a degenerate four wave mixing correlation time gate," *Appl. Opt.* **33** 8346-8353 (1994)
24. M. A. O Leary et al., "Experimental images of heterogeneous turbid media by frequency-domain diffusing-photon tomography," *Opt. Lett.* **20** 426-428 (1995)
25. P. French, "The light fantastic medical show," *New Scientist*, March 11, 25-29 (1995)
26. B. E. A. Saleh and M. C. Teich, *Fundamentals of Photonics*, John Wiley and Sons, Inc., NY, pp136-139 (1991)
27. L. Wang, P. Ho, R. Alfano, "Time-resolved Fourier Spectrum and Imaging in Highly Scattering Media", *Applied Optics*, **32** 5043-8 (1993).
28. L. Wang, P. Ho, X. Liang, R. Alfano, "Fourier-Kerr Imaging in Thick Turbid Media", *Optics Letters*, **18** 241-243 (1993).
29. L. Kalpaxis, L. Wang, X. Liang, P. Galland, P. Ho, R. Alfano, "3D temporal image reconstruction", *Opt. Lett.* **18** 1691-3 (1993)
30. S. G. Demos and R. R. Alfano, "Temporal gating in highly scattering media by the degree of optical polarization," *Opt. Lett.* **21** 161-3 (1996)
31. R. R. Alfano ed. "Optical Biopsy III" *SPIE Vol.3917* (2000)
32. R. R. Alfano, G. C. Tang, Asima Pradhan, W. Lam, D. S. J. Choy, E. Opher, "Fluorescence spectra from cancerous and normal human breast and lung tissues," *IEEE J. Quantum Electron.* **QE-23**, 1806 (1987).
33. C. Kittrel et al., *Applied Optics*, **24**, 2280 (1985).
34. C. H. Liu, W. L. Sha, H. R. Zhu, D. L. Akins, L. Deckelbaum, M. Stetz, K. O'Brien, J. Scott and R. Alfano, "NIR Fourier transform Raman spectroscopy of normal and atherosclerotic human aorta", *Laser in Life Sci.*, **4** 257-261 (1992)
35. W. B. Wang, S. G. Demos, J. Ali, G. Zhang, and R. R. Alfano, "Visibility enhancement of fluorescent objects hidden in animal tissues using spectral fluorescence difference method," *Opt. Comm.* **147** 11-15 (1998)